



ELSEVIER

Physica D 163 (2002) 127–149

PHYSICA D

www.elsevier.com/locate/physd

Dynamical scaling laws in two types of extended Hamiltonian systems at dissipation onset

Chi-Tuong Pham*, Marc Brachet

Laboratoire de Physique Statistique, CNRS UMR 8550, École Normale Supérieure, 24 Rue Lhomond, 75231 Paris Cedex 05, France

Received 3 May 2001; received in revised form 23 October 2001; accepted 3 December 2001

Communicated by A.C. Newell

Abstract

The transition to dissipation in one-dimensional extended Hamiltonian systems with saddle-node bifurcations of stationary solutions is characterized. Three different systems are studied: (i) nonlinear Schrödinger flow past a localized obstacle; (ii) sine-Gordon pendulum chains forced by a local torque; (iii) electrically charged nonlinear Schrödinger flows. In case (i), no frequency gap is present in the dispersion relation. In contrast, in cases (ii) and (iii) a minimum frequency for propagating waves exists. In the gapless case, the growth rates of the unstable modes and the frequency of supercritical soliton emission are found to scale as the square root of the bifurcation parameter. No subcriticality is observed. In contrast, when a frequency gap is present, subcritical soliton emission takes place. Logarithmic and one-fourth power scaling laws are found, respectively, at the bottom and top of the subcriticality window. © 2002 Elsevier Science B.V. All rights reserved.

PACS: 05.45.-a; 02.30.Oz; 67.40.-w; 03.75.Fi

Keywords: Hamiltonian saddle-node bifurcation; Andronov bifurcation; Subcriticality; Dynamical scaling law

1. Introduction

The main motivation of the present work is to try to understand the origin of dynamical scaling laws previously observed in two-dimensional (2D) Hamiltonian systems presenting a local saddle-node bifurcation. These models of superfluidity and Bose–Einstein condensation were considered in the context of the determination of the critical velocity at which superfluidity breaks down. We will proceed by investigating dynamical scaling laws in similar, but much simpler, one-dimensional (1D) Hamiltonian systems. We will thus study the dynamical behavior of three different infinite 1D Hamiltonian systems undergoing spatially localized saddle-node bifurcations. All three systems can radiate waves at infinity. However, they fall in two distinct types. In one type, waves of arbitrarily low temporal frequency can propagate, whereas in the other type, waves can only propagate above a finite cut-off frequency.

Much work has been devoted to the determination of the critical velocity at which superfluidity breaks down [1]. A mathematical model of superfluid ^4He , valid at temperatures low enough for the normal fluid to be negligible, is the nonlinear Schrödinger equation (NLSE), also called the Gross–Pitaevskii equation [2–4]. In a related context, dilute

* Corresponding author.

Bose–Einstein condensates have been recently produced experimentally. These compressible nonlinear quantum fluids are also accurately described by the NLSE allowing direct quantitative comparison between theory and experiment [5]. In a recent experiment, Raman et al. [6] have found a critical Mach number for the onset of dissipation in a Bose–Einstein condensed gas by moving a blue detuned laser beam through the condensate at different velocities.

Studying the 2D superflow around a cylinder, using direct numerical simulations of the NLSE, Frisch, Pomeau and Rica observed a transition to a dissipative regime [7]. They interpreted the results of their simulations in terms of a saddle-node bifurcation of the stationary solutions [8]. Such a saddle-node bifurcation was analytically found by Hakim [9] when studying the stability of 1D NLSE flows across obstacles described by a potential. He obtained explicit expressions for the bifurcating stationary solutions and studied the transitional dynamics. More recently, using numerical continuation techniques, Huepe and Brachet [10,11] were able to obtain the bifurcation diagram corresponding to the 2D superflow around a disc. It was found that the stable (elliptic) branch and the unstable (hyperbolic) branch are connected through a saddle-node bifurcation. Dynamical solutions were studied and the frequency of supercritical vortex shedding was found to scale as the square root of the bifurcation parameter.

In another context, studying dissipative 1D extended systems, Argentina et al. showed that Andronov saddle-node and homoclinic bifurcations [12] can control the dynamical scaling laws [13,14]. In the present work, we will extend to Hamiltonian systems these results obtained in the context of dissipative systems.

The paper is organized as follows. Section 2 is devoted to nonlinear Schrödinger flows past a localized obstacle. After briefly recalling Hakim’s results on the bifurcation of stationary solutions, the unstable eigenmodes and their growth rates are computed using a shooting method and the so-called compound matrix method, described in [15,16]. The dynamical behavior of the system is then investigated using direct numerical simulations. In Section 3, we study sine-Gordon pendulum chains forced by a local torque. The stationary solutions and their bifurcations are obtained analytically. The growth rates of the unstable eigenmodes are also determined analytically. Direct numerical simulations are then performed to characterize the subcritical dynamical behavior. In Section 4, we study the dynamics of an electrically charged nonlinear Schrödinger flow. Finally, Section 5 contains a discussion and our conclusions.

2. Nonlinear Schrödinger flow past an obstacle

2.1. Definition of the system

We consider a point impurity moving at speed v within a 1D superflow. In the frame of the moving impurity, the system can be described by the following action functional

$$\mathcal{A}[\psi, \bar{\psi}] = \int dt \left[\frac{i}{2} \int dx (\bar{\psi} \partial_t \psi - \psi \partial_t \bar{\psi}) - \mathcal{K} \right]. \quad (1)$$

In this expression, ψ is a complex field, $\bar{\psi}$ its conjugate and the energy functional \mathcal{K} reads

$$\mathcal{K} = \mathcal{E} - v\mathcal{P} + v[R^2(+\infty)\phi(+\infty) - R^2(-\infty)\phi(-\infty)], \quad (2)$$

with

$$\mathcal{E} = \int dx \left[|\partial_x \psi|^2 + \frac{1}{2} (|\psi|^2 - 1)^2 + g\delta(x)(|\psi|^2 - 1) \right], \quad (3)$$

$$\mathcal{P} = \int dx \frac{1}{2i} [\bar{\psi} (\partial_x \psi) - \psi (\partial_x \bar{\psi})], \quad (4)$$

$$\psi = R \exp(i\phi). \quad (5)$$

The Dirac (pseudo) potential $g\delta(x)$ in (3) represents the impurity (g parameterizes the strength of this repulsive potential). The last term in (2) imposes the appropriate boundary conditions for the phase ϕ [9]. R obeys the boundary conditions $R^2(\pm\infty) = 1$.

The Euler–Lagrange equation associated to (1), $\delta\mathcal{A}/\delta\bar{\psi} = 0$, is the NLSE

$$i\partial_t\psi = -\partial_{xx}\psi + iv\partial_x\psi - \psi + |\psi|^2\psi + g\delta(x)\psi. \quad (6)$$

We seek continuous solutions of (6) that are differentiable everywhere except at $x = 0$ where they are (spatially) left- and right-derivable. Integrating (6) on an ϵ -neighborhood of $x = 0$ and taking the limit $\epsilon \rightarrow 0$ imposes the discontinuity condition

$$\partial_x\psi(0^+, t) - \partial_x\psi(0^-, t) = g\psi(0, t), \quad (7)$$

thus the $g\delta(x)\psi$ singularity in Eq. (6) is balanced by the $-\partial_{xx}\psi$ term for all times t . Note that the system described by (6) depends on two real parameters v and g . In the following section, we will consider a ξ -indexed family of stationary solutions to (6) where ξ depends continuously on g and v . It will be useful to invert this dependence and consider g as a function of ξ .

2.2. Stationary solutions

Time-independent solutions of the NLSE (6) are best studied by performing the change of variables defined above in (5): $\psi = R \exp(i\phi)$. Using these variables, the NLSE reads

$$\partial_t R = v\partial_x R - R\partial_{xx}\phi - 2\partial_x R\partial_x\phi, \quad (8)$$

$$\partial_t\phi = v\partial_x\phi - (\partial_x\phi)^2 + 1 - R^2 - g\delta(x) + \frac{\partial_{xx}R}{R}, \quad (9)$$

and the jump condition (7) reads

$$\partial_x R(0^+, t) - \partial_x R(0^-, t) = gR(0, t), \quad (10)$$

$$\partial_x\phi(0^+, t) - \partial_x\phi(0^-, t) = 0. \quad (11)$$

Note that Eqs. (8) and (9) can be, respectively, interpreted as the continuity and Bernoulli equations for a fluid of density $\rho = R^2(x)$ and velocity $u = 2\partial_x\phi$ (see, e.g. [17] for details on this interpretation of the NLSE).

Explicit time-independent solutions of Eqs. (8) and (9) were found by Hakim [9], using the so-called gray solitons (a nonlinear optics terminology). Gray solitons [18,19] are stationary solutions of Eqs. (8) and (9), *without* the potential term $g\delta(x)$. They are localized density depletions of the form

$$R_{\text{GS}}^2(x) = \frac{v^2}{2} + \left(1 - \frac{v^2}{2}\right) \tanh^2 \left[\sqrt{\frac{1}{2} - \frac{v^2}{4}} x \right], \quad (12)$$

$$\phi_{\text{GS}}(x) = \arctan \left(\frac{v\sqrt{2-v^2}}{\exp[\sqrt{2-v^2}x] + v^2 - 1} \right). \quad (13)$$

Patching together pieces of gray solitons, Hakim found the following ξ -indexed stationary solutions of Eqs. (8) and (9), *including* the potential term $g\delta(x)$

$$R_\xi(x) = R_{\text{GS}}(x \pm \xi), \quad x \geq 0 \quad (14)$$

$$\phi_\xi(x) = \phi_{\text{GS}}(x \pm \xi) - \phi_{\text{GS}}(\pm \xi), \quad x \gtrless 0, \quad (15)$$

where the jump conditions (10) and (11) impose a value of g corresponding to each value of ξ , via

$$g(\xi) = \sqrt{2} \left(1 - \frac{v^2}{2}\right)^{3/2} \frac{\tanh[\sqrt{1/2 - v^2/4}\xi]}{v^2/2 + \sinh^2[\sqrt{1/2 - v^2/4}\xi]}. \quad (16)$$

The function $g(\xi)$ reaches a maximum $g_c = g(\xi_c)$ at

$$\xi_c = \frac{\text{argcosh}((1 + \sqrt{1 + 4v^2})/2)}{\sqrt{2 - v^2}} \quad (17)$$

with

$$g_c = 4 \left(1 - \frac{v^2}{2}\right) \frac{[\sqrt{1 + 4v^2} - (1 + v^2)]^{1/2}}{2v^2 - 1 + \sqrt{1 + 4v^2}}. \quad (18)$$

The two stationary solutions of (6) corresponding to $\xi_+(g) > \xi_c$ and $\xi_-(g) < \xi_c$ obtained by inverting (16) for $g < g_c$, thus disappear, merging in a saddle-node bifurcation at a critical strength g_c . Note that the bifurcation can also be obtained by varying v and keeping g constant. In the following, the strength g of the delta function is used as the control parameter of our system keeping v constant.

The bifurcation diagram corresponding to the energy \mathcal{K} (see Eq. (2)) is shown as the inset of Fig. 1. The energetically unstable and stable solutions ($\mathcal{K}(\xi_-(g)) > \mathcal{K}(\xi_+(g))$) are also displayed in the figure. Note that the phase $\phi_\xi(x)$, as defined in Eq. (15), differs from that considered in [9] by an (x -independent) constant. The phase in [9] is set to 0 at $x = +\infty$, whereas (15) is antisymmetric in x . This difference is unimportant because Eqs. (8) and (9) are invariant under the constant phase shift

$$\phi(x) \mapsto \phi(x) + \varphi. \quad (19)$$

2.3. Linear stability

We now begin our investigation of dynamical scaling laws by studying the growth rates of unstable eigenmodes close to the bifurcation.

A temporal eigenmode of the form ($e^{\lambda t} r(x)$, $e^{\lambda t} \varphi(x)$) obeys the (second-order in x) ordinary differential equations

$$\lambda r = (v - 2\partial_x \phi_\xi) \partial_x r - \partial_{xx} \phi_\xi r - R_\xi \partial_{xx} \varphi - 2\partial_x R_\xi \partial_x \varphi, \quad (20)$$

$$\lambda \varphi = (v - 2\partial_x \phi_\xi) \partial_x \varphi - 2R_\xi r + \frac{\partial_{xx} r}{R_\xi} - \frac{\partial_{xx} R_\xi}{R_\xi^2} r \quad (21)$$

obtained by linearizing Eqs. (8) and (9) around the stationary solution ($R_\xi(x)$, $\phi_\xi(x)$). The jump conditions (10) and (11) also apply to ($r(x)$, $\varphi(x)$) so that the Dirac- δ singularities in the last two terms of Eq. (21) cancel. Thus the (normalized by $r(0) = 1$) initial data needed to integrate (20) and (21) away from $x = 0^\pm$ is of the form

$$u_0 = \begin{pmatrix} \varphi(0) \\ \frac{d\varphi}{dx}(0) \\ r(0) \\ \frac{dr}{dx}(0^\pm) \end{pmatrix} = \begin{pmatrix} \varphi_0 \\ \varphi'_0 \\ 1 \\ r' \pm \frac{1}{2}g \end{pmatrix}. \quad (22)$$

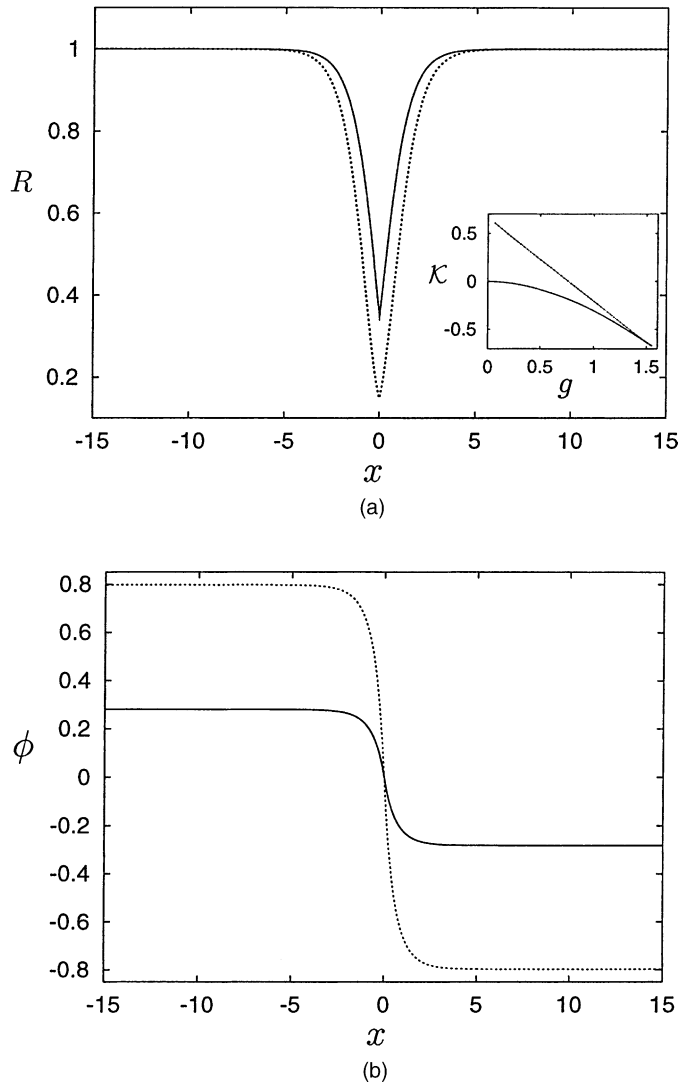


Fig. 1. (a) Modulus R of the stable (—) and unstable (---) stationary solutions of Eq. (6) (see Eq. (14)) for $g = 1.250$ and $v = 0.5$. Insert shows energy functional \mathcal{K} of the stationary solutions versus g for $v = 0.5$ (see Eq. (2)); lower branch—energetically stable branch, upper branch—energetically unstable branch. The bifurcation occurs at $g = 1.5514$. (b) Phase ϕ of the stable (—) and unstable (---) stationary solutions (see Eq. (15)), same conditions as in (a).

Neutral modes, i.e. special solutions of (20) and (21) with $\lambda = 0$, can be obtained analytically. First, the phase shift invariance (19) implies that $(R_\xi(x), \phi_\xi(x) + \Phi)$ is a family of solutions to (8), (9) indexed by the (x -independent) phase Φ . Inserting this family into (20), (21) and taking a Φ -derivative yields the phase neutral mode

$$(r_{\text{PN}}(x), \varphi_{\text{PN}}(x)) = (0, 1). \tag{23}$$

A second (somewhat less trivial) neutral mode is obtained by repeating the above procedure, with the ξ -indexed $(R_\xi(x), \phi_\xi(x))$ family of solutions. Taking a ξ -derivative of (8), (9) with $(R_\xi(x), \phi_\xi(x))$ inserted generates an extra term stemming from the ξ -dependence of g . This extra term is zero at the critical point ξ_c (see Eq. (17)). Thus one

obtains the critical neutral mode $(r_{\text{CN}}(x), \varphi_{\text{CN}}(x)) = (d/d\xi)(R_\xi, \phi_\xi)|_{\xi_c}$ that explicitly reads

$$r_{\text{CN}}(x) = \pm \frac{(2 - v^2)^{3/2} \operatorname{sech}^2(\sqrt{2 - v^2}(x \pm \xi_c)/2) \tanh(\sqrt{2 - v^2}(x \pm \xi_c)/2)}{4\sqrt{1 + (v^2/2 - 1) \operatorname{sech}^2(\sqrt{2 - v^2}(x \pm \xi_c)/2)}} \quad x \gtrless 0, \quad (24)$$

$$\varphi_{\text{CN}}(x) = \mp \frac{v(-2 + v^2) \sinh(\sqrt{2 - v^2}x/2)}{(-1 + v^2 + \cosh(\sqrt{2 - v^2}(x \pm \xi_c)))} \times \frac{\sinh(\sqrt{2 - v^2}(x \pm 2\xi_c)/2)}{(-1 + v^2 + \cosh(\sqrt{2 - v^2}(\xi_c)))} \quad x \gtrless 0. \quad (25)$$

In the following, we restrict our attention to real positive λ . The possible existence of unstable modes with complex growth rate λ is, however, discussed in the last paragraph of this section.

We thus seek growing ($\lambda > 0$) eigenmodes on the (energetically) unstable branch $\xi < \xi_c$. These modes must bear some continuity relation with the above ($\lambda = 0$) neutral modes in the limit $\xi \rightarrow \xi_c$. Further insight is obtained by considering the $x \rightarrow \pm\infty$ asymptotic limit. In this limit, (20) and (21) reduce to the simple homogeneous system

$$\frac{du}{dx} = Mu \quad (26)$$

with

$$u = \begin{pmatrix} \varphi \\ \frac{d\varphi}{dx} \\ r \\ \frac{dr}{dx} \end{pmatrix}, \quad M = \begin{pmatrix} 0 & 1 & 0 & 0 \\ 0 & 0 & -\lambda & v \\ 0 & 0 & 0 & 1 \\ \lambda & -v & 2 & 0 \end{pmatrix}. \quad (27)$$

The characteristic polynomial $\chi_M(\mu) = \det(M - \mu \text{Id})$ reads

$$\chi_M(\mu) = \mu^4 + (v^2 - 2)\mu^2 - 2\lambda v\mu + \lambda^2. \quad (28)$$

Note that formally setting $\mu = ik$ and $\lambda = i\omega$ in (28) yields the dispersion relation

$$\omega = vk + \sqrt{2k^2 + k^4}, \quad (29)$$

which corresponds to sound waves (see [17] and text below Eqs. (8) and (9)).

For small values of $\lambda > 0$, the matrix M has four distinct real eigenvalues, two positive (μ_1^+, μ_2^+) and two negative (μ_1^-, μ_2^-). This property can be extended to finite values of λ in the following way. Calculating the resultant (see, e.g. [20]) of χ_M and its μ -derivated polynomial χ'_M , $P_R = \text{Res}(\chi_M, \chi'_M)$ yields

$$P_R = 16\lambda^2(16\lambda^4 - 2(-2 + v^2)^3 + \lambda^2(-32 - 40v^2 + v^4)). \quad (30)$$

The polynomial $\chi_M(\mu)$ admits multiple roots if and only if $P_R = 0$. Solving this equation yields the λ -roots,

$$\lambda_1^\pm = \pm \sqrt{1 + \frac{5v^2}{4} - \frac{v^4}{32} - \frac{v(16 + v^2)^{3/2}}{32}} \quad \lambda_3 = 0 \quad (\text{of multiplicity } 2), \quad (31)$$

$$\lambda_2^\pm = \pm \sqrt{1 + \frac{5v^2}{4} - \frac{v^4}{32} + \frac{v(16 + v^2)^{3/2}}{32}}. \quad (32)$$

For all $0 \leq v < \sqrt{2}$, the λ -roots verify $0 \leq \lambda_1^+ \leq \lambda_2^+$. Therefore, for fixed v and for real values of $\lambda \in]0, \lambda_1^+[$, $\mu_{1,2}^\pm$ are real and distinct. In this finite λ interval, M is thus diagonalizable, with eigenvectors (u_1^+, u_2^+) and (u_1^-, u_2^-) .

In order to be bounded, solutions to (20), (21) on the whole real axis must therefore have components in the eigenvector basis ($u_{1,2}^\pm$) that vanish in the limits $x \rightarrow \pm\infty$. This condition, applied to the *spatially* growing eigenvectors, yields four nontrivial asymptotic conditions.

To find the unstable eigenmodes, we have developed a shooting method that works as follows. At a given position $\xi < \xi_c$ (see Eq. (17)) on the unstable branch, four numbers must be specified to solve (20) and (21): the initial data $\varphi_0, \varphi'_0, r', r''$ (22) and the growth rate λ . Starting with an initial guess, we numerically integrate (20) and (21) on the interval $-A < x < A$. The solution vector is then expressed in the eigenvector basis at $x = \pm A$. The “errors”, i.e. the component of the solution on the (spatially growing) subspaces $\text{Span}(v_1^-, v_2^-)$ at $x = -A$ and $\text{Span}(v_1^+, v_2^+)$ at $x = +A$, are then computed. Newton–Raphson [21] iterations are performed in order to drive the errors to zero by modifying the values of the initial data vector and eigenvalue λ . This procedure provides the eigenfunctions ($r(x), \varphi(x)$) on the interval $-A < x < A$. The components of the solution on the spatially decaying eigenvectors at $x = \pm A$ and the exact (exponential) solutions of Eq. (26) are used to extend ($r(x), \varphi(x)$) beyond $x = \pm A$. The initial guess needed to start the procedure is obtained by spatially discretizing (20) and (21) and diagonalizing the corresponding (large) matrix. The results reported below were obtained with $A = 8$. We have checked (data not shown) that they were insensitive to the precise value of A .

Practically, this shooting method was found to work correctly only close to the bifurcation. It is well known that the problem of integrating individual vectors of an unstable manifold of dimension greater than 1 is a highly ill-posed problem numerically [22]. There is, however, a simple way to numerically integrate this equation in a robust and stable way. This so-called compound matrix method is described in detail in [15,16]. The method furnishes the eigenvalue as the zero of the so-called Evans function. A key element is the use of exterior algebra which takes as basis vectors 2D subspaces. We have implemented this method, and found it to work reliably, everywhere on the unstable branch.

The growth rates, corresponding to $v = 1/2$, obtained both by the compound matrix method and the shooting method, are displayed in Fig. 2 together with the eigenmodes (only available in the framework of the shooting method). It is apparent, by inspection of Fig. 2(a), that the growth rate λ admits a maximum $\lambda_{\max} \simeq 0.263$. Note that $\lambda_{\max} < \lambda_1^+ \simeq 0.536$. Thus, for all computed values of λ , the M matrix eigenvectors ($u_{1,2}^\pm$) form a nondegenerate basis (see discussion below Eq. (32)). The asymptotic conditions used for both the shooting and compound matrix methods are therefore consistent. Note that the growth rates determined by both methods are in very good agreement.

The growth rate is seen to approach 0 when $\xi \rightarrow 0$. In this limit $g(\xi) = 0$ (see Eq. (16)) and the stationary solution (14) and (15) reduces to a gray soliton. Note that gray solitons are known to be *stable* solutions of Eqs. (8) and (9) (with $g = 0$) [23]. It is therefore natural that the growth rate λ vanishes in this limit.

It is apparent in Fig. 2 that the growth rate λ also vanishes at the bifurcation, linearly with $\xi - \xi_c$. Note that this linear scaling implies a $|g - g_c|^{1/2}$ scaling for the characteristic growth time on the unstable branch (see Eq. (16)). By inspection of Fig. 2, the eigenmodes are seen to converge towards the neutral mode. However, the convergence of the phase is nonuniform in x . This behavior can be understood by the following considerations. Taylor expanding the roots of (28), one obtains explicit formulas that read, for $v = 0.5$,

$$\mu_1^+(\lambda) = \frac{\sqrt{7}}{2} + \frac{2\lambda}{7} + \mathcal{O}(\lambda^2), \quad \mu_2^+(\lambda) = \frac{2(2\sqrt{2} - 1)}{7}\lambda + \mathcal{O}(\lambda^3), \quad (33)$$

$$\mu_1^-(\lambda) = \frac{-\sqrt{7}}{2} + \frac{2\lambda}{7} + \mathcal{O}(\lambda^2), \quad \mu_2^-(\lambda) = \frac{-2(1 + 2\sqrt{2})}{7}\lambda + \mathcal{O}(\lambda^3). \quad (34)$$

For $\lambda > 0$, the spatial growth rates μ_2^\pm tend to 0, but are finite. Consequently, for $\lambda \neq 0$, the phase of the eigenmodes converges towards 0 at $x = \pm\infty$, whereas the neutral ($\lambda = 0$) mode (Eq. (25)) has a finite phase shift.

Note that the eigenmodes found on the unstable branch cannot pass to the stable branch by simple analytical continuation. Indeed, replacing the unstable eigenvalue λ_U by $\lambda_S = i\lambda_U$ for the resolution of (26) around the

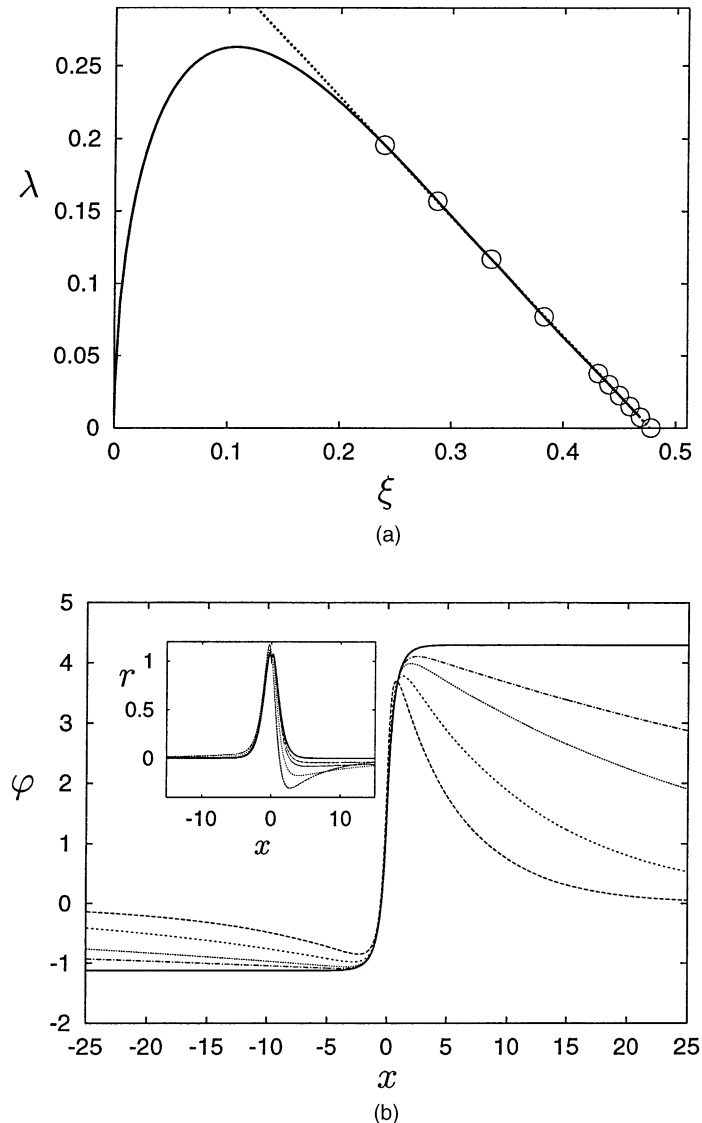


Fig. 2. Solutions to the linear stability equations (20) and (21). (a) Growth-rate λ versus ξ for $v = 0.5$. (—) Compound matrix method of [15,16]; (○) shooting method described below Eq. (29). (b) Phase φ of the unstable mode for $\xi = 0.287, 0.382, 0.440, 0.459$ and 0.478 ; insert: modulus r of the unstable mode. The symmetric r (—) is the neutral mode (Eq. (24)). Note the nonuniformity of the convergence towards the phase of the neutral mode (Eq. (25)) and the linear scaling of the growth rate λ (see text).

stable branch yields the four eigenvalues (33) and (34), with purely imaginary λ_S . Bounded eigenmodes require 0 components on the eigenvector corresponding to $\mu_1^+(i\lambda_U)$ at $+\infty$ and $\mu_1^-(i\lambda_U)$ at $-\infty$, the two other components remaining bounded. Thus, in contrast with the unstable branch, two degrees of freedom remain free in the choice of the eigenmode. Therefore, we can expect in this case a continuum of nonlocalized oscillating eigenmodes. We have not attempted to compute such modes.

We now turn to a discussion of the possible existence of unstable modes with complex growth rate λ . Our main focus in the present work is to understand the dynamical scaling laws occurring on the unstable branch near the

bifurcation ($\xi \rightarrow \xi_c$). In this limit, the shape of the Evans function (data not shown) suggest the existence of a single real isolated eigenvalue. The numerical simulations (see next section) strongly suggest a dominant real eigenvalue. However, although we have found no indication of unstable modes with complex growth rate, we cannot rule out their existence. The problem of the complete determination of the spectrum of Eqs. (8) and (9), including complex eigenvalues is left for further studies.

2.4. Dynamical results

In this section, we study the dynamics of the system near the stationary solutions and in the supercritical regime, by numerical integration of Eq. (6).

Spatial derivatives are evaluated with a centered second-order finite difference scheme. Time stepping is performed using the semi-implicit leapfrog Crank–Nicholson scheme

$$\frac{i(\psi_{n+1} - \psi_{n-1})}{\Delta t} = L_{n+1} + L_{n-1} + 2NL_n, \quad (35)$$

where L_n and NL_n stand, respectively, for the linear and nonlinear parts of the right-hand side of Eq. (6) evaluated for $\psi_n = \psi(t_0 + n\Delta t)$. The computations reported below were performed with space discretization $\Delta x = 0.005$ and time discretization $\Delta t = 0.001$.

We checked that the numerical scheme reproduced the linear stability results of Section 2.3 by studying the growth of a perturbation near the unstable branch. At $v = 0.295$ and $g = 3$, the linear stability result is $\lambda = 0.07827$, and numerical integration yields $\lambda^{\text{num}} = 0.0803$. We have checked (data not shown) that this 2.5% error is due to space discretization.

As observed by Hakim [9], an initial condition equal to an analytic unstable stationary solution relaxes towards the stable solution releasing gray solitons upstream and downstream.

In order to characterize the dynamical behavior, we studied small perturbations around the stable stationary solutions. We found that they decay exponentially in time by emitting sound waves. The characteristic decay time, that diverges with the scaling law $T \sim |g - g_c|^{-1/2}$ at the bifurcation, is plotted in Fig. 3. Note that this exponential decay (instead of oscillations) is rather surprising for a reversible system. However, far from $x = 0$, the dispersion relation (29) holds. This means that sound waves can be emitted at arbitrary low frequency. Thus, the emission of sound waves appears to damp the system.

Finally, we studied the system in the supercritical regime $g > g_c$. We found, as already observed in [9], a transition to dissipation where the system starts emitting periodically in time solitons that move away upstream and downstream. We found that the characteristic time of the period T of soliton emission diverges with the scaling law $T \sim |g - g_c|^{-1/2}$ (see Fig. 3). No hysteresis has been encountered. Note that this behavior is typical of an Andronov saddle-node bifurcation occurring when there exists a homoclinic connection at the bifurcation point [12].

2.5. Discussion

One of the main results found in the previous sections is the scaling law $|\delta|^{-1/2}$ for all the characteristic times close to the bifurcation ($\delta = (g_c - g)/g_c$). Note that this scaling was previously found for supercritical vortex shedding in 2D NLSE flow [11]. This scaling is generic of the (first-order in time) saddle-node bifurcation with normal form

$$m_{\text{eff}} \dot{Q} = \beta Q^2 - \delta. \quad (36)$$

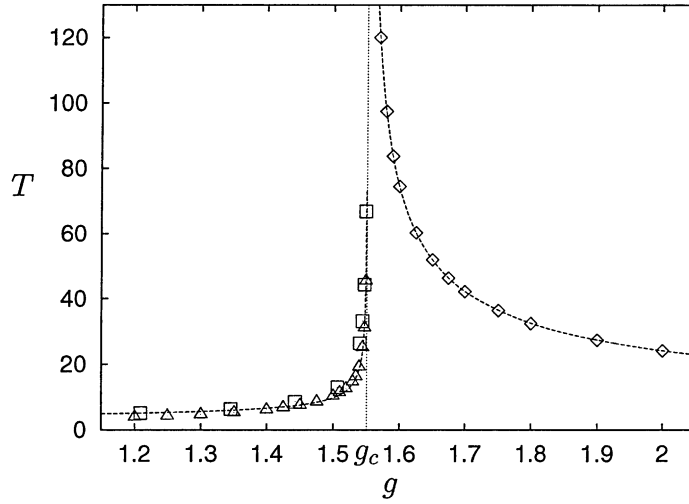


Fig. 3. Dynamical scalings close to the threshold ($g_c = 1.551404$, $v = 0.5$). (\square) Growth characteristic time $T = 1/\lambda$ (see Fig. 2(a)) on the unstable branch, (Δ) relaxation time on the stable branch, (\diamond) period of gray soliton emission. The curves represent fits with scaling law $|g - g_c|^{-1/2}$.

Indeed, looking for solutions of the form $Q = Q_0 + \epsilon$ ($Q_0 = \pm(\delta/\beta)^{1/2}$ are stationary solutions) yields by linearization $m_{\text{eff}}\dot{\epsilon} = \pm 2(\beta\delta)^{1/2}\epsilon + o(\epsilon)$. Thus, the characteristic time scales as $\lambda \sim \delta^{-1/2}$.

The normal form (36) and its associated scaling are rather unexpected in a Hamiltonian system. When we studied the eigenvalues and the eigenmodes of the system, we found that the unstable eigenmode disappears at the bifurcation, merging in a continuum of oscillating eigenmodes (see discussion in the last paragraph of Section 2.3). It is possible that this behavior is at the origin of the $\delta^{1/2}$ scaling.

One way to check this hypothesis is to avoid the merging of the unstable mode into a continuum. This can be done by including a frequency gap in the dispersion relation of the system (see the simple model discussed in Section 5.1). In the remainder of the paper, we thus consider models with this property.

3. Sine-Gordon pendulum chain forced by a local torque

3.1. Definition of the system

In this section, we study a system described by the following action

$$\mathcal{A}[\phi] = \int dt \left[\int dx \frac{1}{2} (\partial_t \phi)^2 - \mathcal{E} \right]. \quad (37)$$

In this equation, ϕ is a real field and the energy functional \mathcal{E} reads

$$\mathcal{E}[\phi] = \int dx \left[\frac{1}{2} (\partial_x \phi)^2 + (1 - \cos \phi) - \alpha \delta(x) \right]. \quad (38)$$

The Euler–Lagrange equation associated to (37), $\delta\mathcal{A}/\delta\phi = 0$, yields the sine-Gordon equation

$$\partial_{tt}\phi - \partial_{xx}\phi + \sin \phi - \alpha \delta(x) = 0, \quad (39)$$

with boundary conditions: $\lim_{x \rightarrow \pm\infty} \partial_x \phi(x) = \lim_{x \rightarrow \pm\infty} \phi(x) = 0$, where the discontinuity condition

$$\partial_x \phi(0^+, t) - \partial_x \phi(0^-, t) = -\alpha \quad (40)$$

is imposed in order to balance the $\alpha \delta(x)$ singularity at all times t .

This system can be pictured as the continuous limit of an infinite chain of coupled pendulum of momentum of inertia I , with the n_0 th pendulum forced by an external torque Γ_{ext} . Note that one could realize this system experimentally by fixing a pulley and a weight to the forced pendulum. The forced pendulum should be modified in order to keep the total inertia momentum (including weight and pulley) equal to I . Thus, the equation of motion for pendulum n reads

$$\frac{d^2 \theta_n}{dt^2} = c_0^2 (\theta_{n+1} + \theta_{n-1} - 2\theta_n) - \omega_0^2 \sin \theta_n + \frac{\Gamma_{\text{ext}}}{I} \delta_{n,n_0}, \quad (41)$$

with $\omega_0^2 = mgL/I$ and $c_0^2 = \beta/I$, where m is the mass of the pendulum, g the acceleration due to gravity and β the coupling constant between the pendula; $\delta_{n,n_0} = 1$ if $n = n_0$, and 0 otherwise. The continuous limit (39) is obtained by setting $\omega_0^2 = 1$, $c_0^2 = 1/\Delta x^2$ and $\Gamma_{\text{ext}}/I = \alpha/\Delta x$.

Note that for $\alpha = 0$, one obtains, by linearization around $\phi = 0$ a dispersion relation with gap: $\omega^2 = \omega_0^2 + c_0^2 k^2$. Thus the pendulum chain cannot propagate waves at frequencies lower than ω_0 .

3.2. Stationary solutions

Stationary solutions of (39) *without* the delta function (known as kink and anti-kink solitons) can be easily calculated [24], they read

$$\phi_{\text{K}/\bar{\text{K}}}(x) = 4 \arctan \exp(\pm x). \quad (42)$$

Patching together pieces of kink and anti-kink solitons yields the following ξ -indexed stationary solutions of (39) *including* the delta function

$$\phi_{\xi}(x) = 4 \arctan \exp[\xi \mp x], \quad \text{if } x \geq 0, \quad (43)$$

where the jump condition (40) imposes the relation

$$\alpha(\xi) = \frac{4}{\cosh(\xi)}. \quad (44)$$

This function reaches a maximum $\alpha_c = 4$ at $\xi = 0$. Thus, for $\alpha < 4$, $\alpha(\xi)$ can be inverted as

$$\xi_{\pm} = \pm \text{argcosh} \left(\frac{\alpha_c}{\alpha} \right). \quad (45)$$

The two stationary solutions $\phi_{\xi_{\pm}}(x)$ disappear at $\alpha = \alpha_c$, merging in a saddle-node bifurcation. The energy of the stationary solutions $\phi_{\xi_{\pm}}(x)$ can be computed using (38), yielding

$$\mathcal{E}[\phi_{\xi_{\pm}}] = 8(1 + \tanh \xi_{\pm}) - \alpha \phi_{\xi_{\pm}}(0), \quad (46)$$

with $\phi_{\xi_-}(0) = 2 \arcsin(\alpha/\alpha_c)$ and $\phi_{\xi_+}(0) = 2\pi - 2 \arcsin(\alpha/\alpha_c)$. The bifurcation diagram is displayed in Fig. 4, where the stationary solutions ϕ_{ξ_-} and ϕ_{ξ_+} are seen to be energetically stable and unstable, respectively.

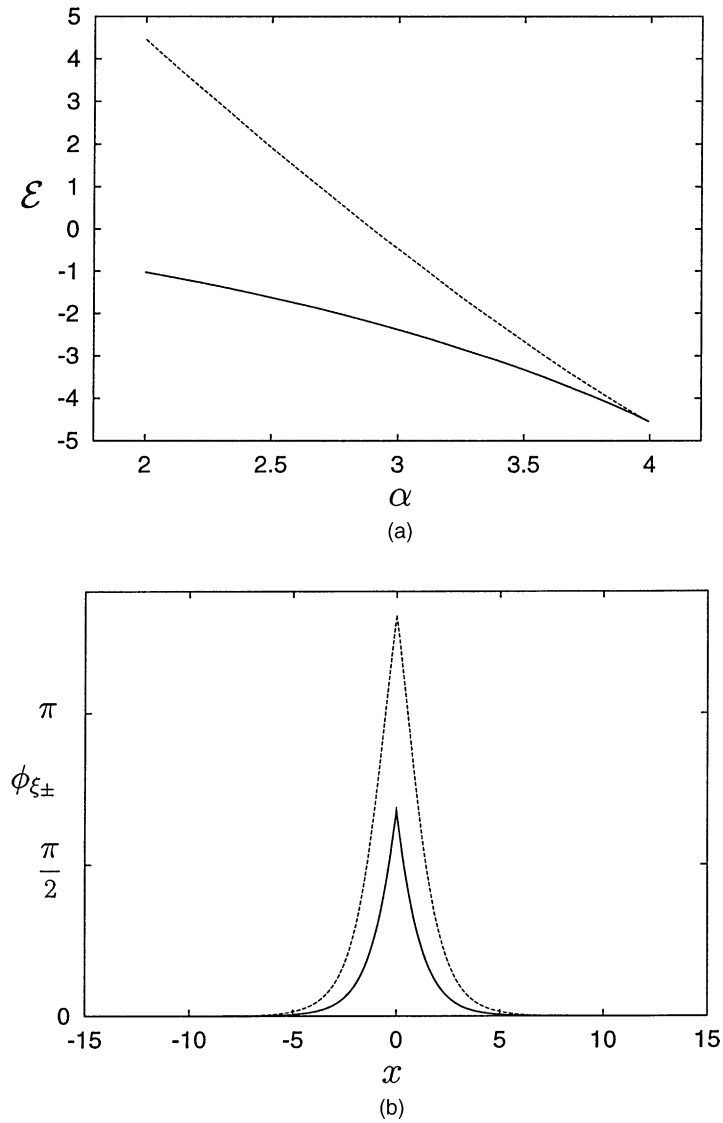


Fig. 4. (a) Plot of the energy functional \mathcal{E} (see Eq. (46)) of the stationary solutions to Eq. (39) versus α . Lower branch— $\mathcal{E}[\phi_{\xi_-}]$, upper branch— $\mathcal{E}[\phi_{\xi_+}]$. (b) Stable (—) and unstable (---) stationary solutions corresponding to $\alpha = 3.5$.

3.3. Linear stability

Linearizing (39) around the time-independent solutions (43) for a perturbation of the form

$$\phi(x, t) = \phi_{\xi}(x) + \epsilon \psi(x) e^{i\omega t} \tag{47}$$

yields the equation

$$\omega^2 \psi + [\partial_{xx} + (2 \operatorname{sech}^2(\xi \mp x) - 1)]\psi = 0, \quad \text{for } x \geq 0. \tag{48}$$

Taking the ξ -derivative of (43) at $\xi = 0$, in exactly the same way as in Section 2.3, provides the neutral ($\omega^2 = 0$) mode

$$\psi_0(x) = 2 \operatorname{sech}(x). \quad (49)$$

Note that $f(y) = \exp(\sqrt{1 - \omega^2}y)[\sqrt{1 - \omega^2} - \tanh y]$ is a solution to $\omega^2 f + [\partial_{yy} + (2 \operatorname{sech}^2 y - 1)]f = 0$. Setting, for $x < 0$, $y = x + \xi$ and symmetrizing around $x = 0$ yields the (arbitrarily normalized) exact solution to (48)

$$\psi_\xi(x) = e^{\sqrt{1 - \omega^2}(\xi \mp x)} [\sqrt{1 - \omega^2} - \tanh(\xi \mp x)], \quad \text{for } x \gtrless 0, \quad (50)$$

$$\omega^2 = \frac{1}{2} \tanh^2 \xi \left[1 - \sqrt{\cotanh^2 \xi + 3 \operatorname{cosech}^2 \xi} \right], \quad (51)$$

where (51) is obtained by imposing $(d\psi_\xi(x)/dx)|_{x=0} = 0$.

The function $\omega^2(\xi)$ together with selected eigenmodes $\psi(x)$ are displayed in Fig. 5. One can note that ω^2 has a unique minimum ω_{\min}^2 that can be computed by solving $d\omega^2/d\xi = 0$ which yields $\xi_{\min} = \operatorname{argsech} \sqrt{2/3}$ corresponding to $\omega_{\min}^2 = -1/3$ and $\alpha_{\min} = 4\sqrt{2/3}$.

The asymptotic behavior $\lim_{\xi \rightarrow -\infty} \omega^2 = 1^-$ and $\lim_{\xi \rightarrow +\infty} \omega^2 = 0^-$ can be understood by the following considerations. Around the stable branch, far from the bifurcation, the stationary solution approaches a pendulum chain at rest. A global oscillation of the chain corresponds to $\omega^2 = 1$. Around the unstable branch, far from the bifurcation, the stationary solution tends to a pair of infinitely distant static kink and anti-kink. The neutral mode that changes the distance between kink and anti-kink corresponds to $\omega^2 = 0$.

At the bifurcation, the eigenmodes are localized, and one can continuously pass from the unstable eigenmode to the stable eigenmode. These eigenmodes have a similar shape in contrast with the situation of Fig. 2.

Near $\xi = 0$, Eq. (51) yields $\omega^2 = -\xi + o(\xi)$. As (see Eq. (45)) $\xi_\pm = \pm\sqrt{2}\delta^{1/2} + o(\delta^{1/2})$, with $\delta = (\alpha_c - \alpha)/\alpha_c$, we can conclude that

$$\omega^2 = \mp\sqrt{2}\delta^{1/2} + o(\delta^{1/2}). \quad (52)$$

Note that this scaling implies a $|\alpha - \alpha_c|^{-1/4}$ scaling for the period of oscillations on the stable branch and for the characteristic growth time $2\pi/|\omega|$ on the unstable branch. Moreover, these scalings are typical of a Hamiltonian saddle-node bifurcation (see Section 3.5).

3.4. Dynamical results

In this section, we study the dynamics of the system near the stationary solutions by numerical integration of Eq. (39).

Spatial derivatives are calculated with a centered second-order finite difference scheme. Time stepping is performed using a fourth-order Runge–Kutta algorithm. The computations reported below were performed with spatial and temporal discretization $\Delta x = 0.01$ and $\Delta t = 0.0002$.

We checked that the numerical scheme reproduced the linear stability results of Section 3.3, by studying the dynamics of a perturbation near the unstable and stable branch. We found very good agreement. For instance, on the stable branch at $\omega^2 = 0.3$ and $\xi = -0.2778$ (see Fig. 5) corresponding to $\alpha(\xi) = 3.64$ (Eq. (44)), the numerical integration yields $\omega_{\text{num}}^2 = 0.301$. The error, lower than 1%, is due to space discretization.

At subcritical values of α , initial conditions, close to the analytical unstable stationary solutions, relax towards stable solutions, releasing to infinity a kink/anti-kink pair. In the supercritical regime $\alpha > \alpha_c$, the system exhibits a transition to dissipation: kink/anti-kink pairs are periodically emitted (data not shown).

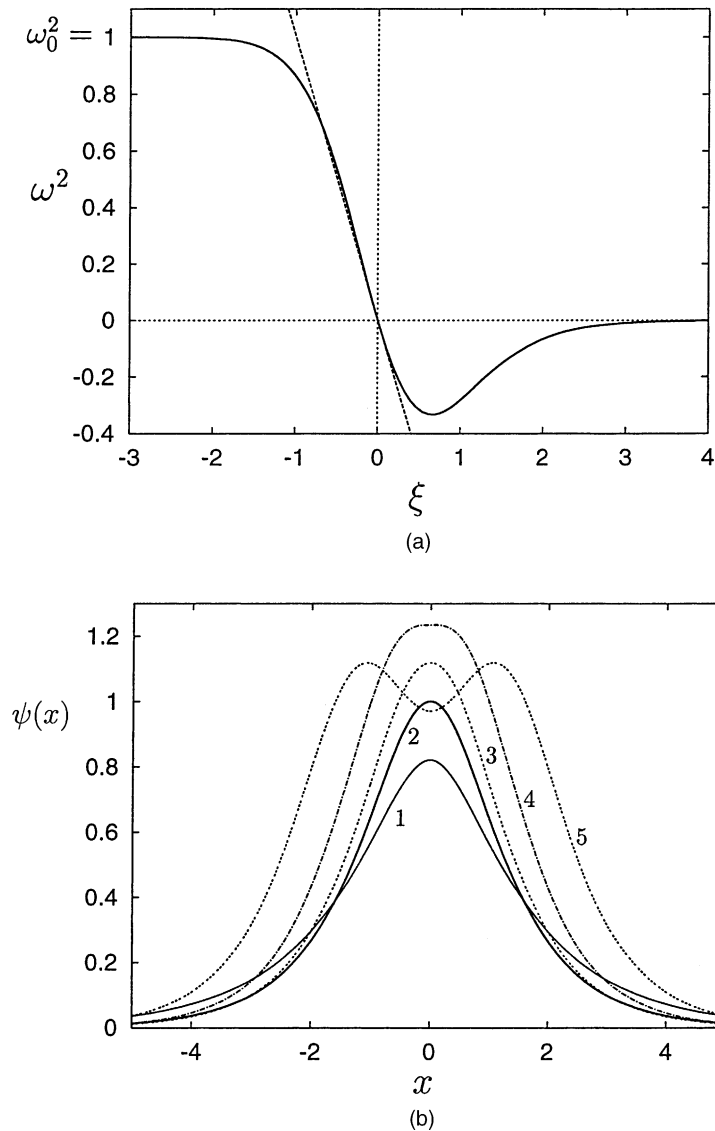


Fig. 5. (a) Plot of ω^2 versus the shift parameter ξ (see Eq. (51)). Note the existence of a minimum ω_{\min}^2 ; (b) stable mode (curve 1, $\omega^2 = 0.5$), neutral mode (curve 2, $\omega^2 = 0$) and unstable modes (curves 3, 4 and 5) corresponding, respectively, to $\omega^2 = -0.2$, ω_{\min}^2 and -0.2 . Note that curves 3 and 5 correspond to two different values of ξ with the same value of ω^2 .

Considering the pendulum chain is an easy way to understand these phenomena. For strong enough external torques, the forced pendulum passes the value π . It then makes a rotation of 2π , while dragging the pendulum chain. In this way, the system emits periodically pairs of kink/anti-kink, radiating energy to infinity. Note that the energy supplied by the work of the forced pendulum, $E_S = 8\pi$, is larger than that of a pair of static kink/anti-kink, $E_0 = 16$. By energy conservation, the velocity of a pair of solitons is finite.

A striking result, displayed in Fig. 6, is that this periodic regime exhibits subcriticality. Starting in the supercritical ($\alpha > \alpha_c$) regime and decreasing α , we found that the system continues to emit solitons down to $\alpha = \alpha'_c = 3.888$.

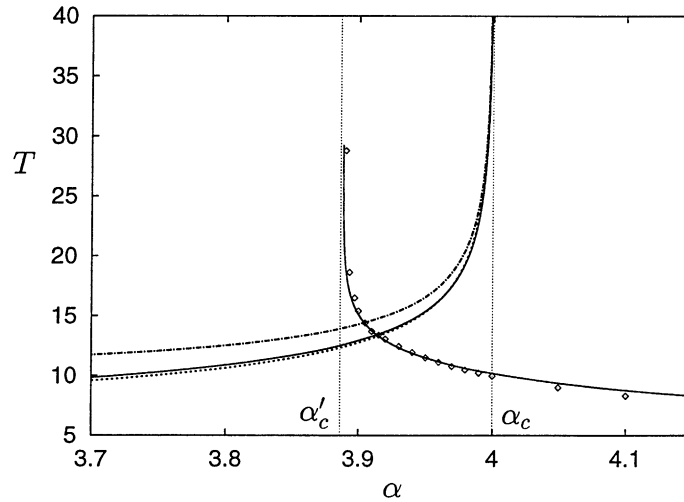


Fig. 6. Dynamical scalings close to the threshold ($\alpha_c = 4$). (— · —) Growth characteristic time $2\pi/|\omega|$ on the unstable branch, (---) period of oscillations around the stable branch, see Fig. 5(a), (\diamond) period of kink/anti-kink emission. The solid curves represent fits with scaling laws $|\alpha - \alpha_c|^{-1/4}$ and $\log(\alpha - \alpha'_c)$, see text below Eq. (53).

The period of soliton emission diverges when α approaches α'_c . Below α'_c , the system relaxes near the stable solution after emitting only one pair of kink/anti-kink. Note that at $\alpha = \alpha'_c$, the energy supplied by the external torque is again larger than the energy of a pair of static kink/anti-kink. Thus the spatial and temporal periods of kink/anti-kink both diverge at α'_c , while their velocity of emission remains finite. We checked (data not shown) that the value of α'_c was insensitive to Δx .

One mechanism for subcriticality is the homoclinic Andronov bifurcation [12], which is a global bifurcation. In phase space, the unstable stationary solutions are fixed points characterized by a 1D unstable manifold and a one-codimensional stable manifold. The homoclinic Andronov bifurcation occurs when the unstable manifold connects back to the stable manifold, forming a homoclinic connection. After the bifurcation, the connection disappears leaving a limit cycle. Near the bifurcation, the characteristic time scales as

$$T = -\frac{1}{\lambda_+} \log(\alpha - \alpha'_c) + o(\log(\alpha - \alpha'_c)), \quad (53)$$

where λ_+ is the value of the unstable eigenvalue of the system at α'_c . This bifurcation has been found in extended dissipative models [13].

We have measured the period of emission of the solitons and fitted it with the scaling law $T = \tau + (1/\lambda_{SL}) \log(\alpha - \alpha'_c)$ with $\alpha'_c = 3.888$, $\lambda_{SL} = 0.454$ and $\tau = 15.5$, see Fig. 6. The value of λ_+ (see Fig. 5(a)) is 0.450, thus λ_{SL} and λ_+ differ by less than 1%.

This very good agreement together with the quality of the fit displayed in Fig. 6 is a strong argument in favor of the Andronov homoclinic bifurcation as the mechanism for subcriticality in our system. Note that to the best of our knowledge, it is the first time that such a bifurcation has been found in an extended Hamiltonian system.

3.5. Discussion

We have just seen that the presence of a gap in the dispersion relation yields a continuity in the eigenmodes at the bifurcation and is responsible for a hysteresis phenomenon. We found at the top of the subcriticality window

($\alpha = \alpha_c$) a scaling law for the unstable eigenvalues of the linear problem of the type $\lambda_U \sim (\alpha_c - \alpha)^{1/4}$. This scaling can be obtained from the normal form of the Hamiltonian saddle-node bifurcation

$$m_{\text{eff}} \ddot{Q} = \beta Q^2 - \delta, \quad (54)$$

using the same arguments as in Section 2.5.

The parameters appearing in (54) can be determined by the following considerations. Writing the normal form as $\ddot{Q} = -\partial V / \partial Q$, where $V(Q, \delta) = \beta(Q^3/3) - \delta Q + V_0 + \lambda\delta$, the stationary solutions are $Q_{\pm} = \pm(\delta/\beta)^{1/2}$. Thus

$$V(Q_{\pm}, \delta) = \pm \frac{2\delta^{3/2}}{3\beta^{1/2}} + V_0 + \lambda\delta. \quad (55)$$

Comparing (55) with, on the one hand the asymptotic development of (46)

$$\mathcal{E}(\phi_{\xi_{\pm}}) = 4[2 - \pi + \pi\delta \pm \frac{4}{3}\delta^{3/2}], \quad (56)$$

where $\delta = (\alpha_c - \alpha)/\alpha_c$, and on the other hand, with Eq. (52), yields $m_{\text{eff}} = 1$ and $\beta = 1/2$. This normal form could also be explicitly computed by making use of a collective coordinate approach of the type given in [25].

The gap appears to open a subcriticality window, with a Hamiltonian saddle-node bifurcation on top and an Andronov bifurcation at the bottom. Note that the Andronov homoclinic bifurcation responsible for subcriticality, being a global bifurcation, cannot be obtained in the above context of local bifurcation theory.

In order to verify the generality of this subcritical behavior, we have tried to make the simplest modification of Eq. (6) opening a frequency gap in the dispersion relation.

4. Electrically charged nonlinear Schrödinger flow

4.1. Definition of the system

In this section, we consider the system defined by the following action

$$\mathcal{A}[\psi, \bar{\psi}, V] = \int dt \left[\frac{i}{2} \int dx (\bar{\psi} \partial_t \psi - \psi \partial_t \bar{\psi}) - \mathcal{K}' \right], \quad (57)$$

where ψ is a complex field, $\bar{\psi}$ its conjugate, V a real field and \mathcal{K}' the energy functional of the system, equal to \mathcal{K} in (2) with a supplementary term

$$\mathcal{K}' = \mathcal{K} + \int dx \left[qV(|\psi|^2 - \langle |\psi|^2 \rangle) \frac{1}{2} (\partial_x V)^2 \right]. \quad (58)$$

$\langle |\psi|^2 \rangle$ is the (spatial) mean value of $|\psi|^2$, equal to 1 in an infinite system. The Euler–Lagrange equations, $\delta \mathcal{A} / \delta \bar{\psi} = 0$ and $\delta \mathcal{A} / \delta V = 0$, yield the following NLSE

$$i \partial_t \psi = -\partial_{xx} \psi + iv \partial_x \psi - \psi + |\psi|^2 \psi + g \delta(x) \psi + qV\psi, \quad (59)$$

$$\partial_{xx} V = -q(|\psi|^2 - \langle |\psi|^2 \rangle). \quad (60)$$

This system can be viewed as a charged 1D superflow past an obstacle, the electrostatic field created by the charged flow interacting with the latter [26]. It is also the dynamical equation for a 1D superconductor in the presence of an impurity given in [27]. We have chosen to use as a source term $|\psi|^2 - \langle |\psi|^2 \rangle$ in order to insure global charge neutrality so that $0 = \nabla V(+\infty) = \nabla V(-\infty)$.

The dispersion relation of the system away from the obstacle can be found considering that $qV = U$ is a nonlocal term in the action ($qV = q^2 \Delta^{-1} [|\psi|^2 - \langle |\psi|^2 \rangle]$). It is shown in [28] that this potential adds a supplementary term in the dispersion relation of the form

$$\omega = vk + \sqrt{k^2 \hat{U}(k) + 2k^2 + k^4},$$

where $\hat{U}(k)$ is the Fourier transform of U . As $\hat{U}(k) = q^2/k^2$, the electrostatic field adds a gap with cut-off frequency $\omega_c = q$ to the dispersion relation

$$\omega = vk + \sqrt{\omega_c^2 + 2k^2 + k^4}. \quad (61)$$

No sound wave can therefore propagate at frequencies lower than ω_c .

4.2. Stationary solutions

We were unable to find the stationary solutions analytically for $q \neq 0$. A simple way to numerically obtain stable stationary solutions of (59), at fixed g , v and q , is to let the system relax, following the Ginzburg–Landau equation, $\partial_t \psi = \delta \mathcal{K}' / \delta \bar{\psi}$

$$\partial_t \psi = \partial_{xx} \psi - iv \partial_x \psi + \psi - |\psi|^2 \psi - g \delta(x) \psi - qV \psi, \quad (62)$$

$$\partial_{xx} V = -q(|\psi|^2 - \langle |\psi|^2 \rangle). \quad (63)$$

Note that the stationary solutions of (62) are identical to those of (59). This procedure does not yield unstable solutions.

However, g in (3) is a Lagrange multiplier that imposes the value of $|\psi(0)|^2$. We can instead directly impose $|\psi(0)| = R_0$, while minimizing $\mathcal{K}'_0 = \mathcal{K}'|_{g=0}$. This is equivalent to integrating (62) with $g = 0$ and boundary condition $|\psi(0)| = R_0$, then to compute, through (7), the corresponding value of g . The bifurcation diagram and the stationary solutions obtained by this procedure are displayed in Fig. 7.

It can be seen by inspection of the figure that, unlike the stationary solutions of the case $q = 0$, the charged stationary solutions have two bumps on both sides of the discontinuity. This is due to Coulombian screening that tends to accumulate positive charges near the depletion that stands at the discontinuity. The bifurcation diagram of \mathcal{K}' shows that the upper branch of \mathcal{K}' is energetically unstable.

4.3. Linear stability

As explained in Section 2.3, the neutral mode is obtained by taking the derivative of the family of the stationary solutions with respect to a regular parameter, at the bifurcation. We thus evaluate the neutral mode as

$$\frac{\psi(R_0 + \Delta R_0) - \psi(R_0 - \Delta R_0)}{2\Delta R_0},$$

where $\psi(R_0 \pm \Delta R_0)$ are the stationary states calculated at modulus $R_0 \pm \Delta R_0$. The phase and the modulus of the neutral mode obtained by this procedure are plotted in Fig. 8. It can be seen in the figure that the neutral mode has a finite phase shift.

We have also integrated slightly perturbed stationary solutions in order to obtain the linearly stable and unstable modes. The growing and oscillatory modes are found to have very similar shapes (see Fig. 8). These modes have a finite phase shift.

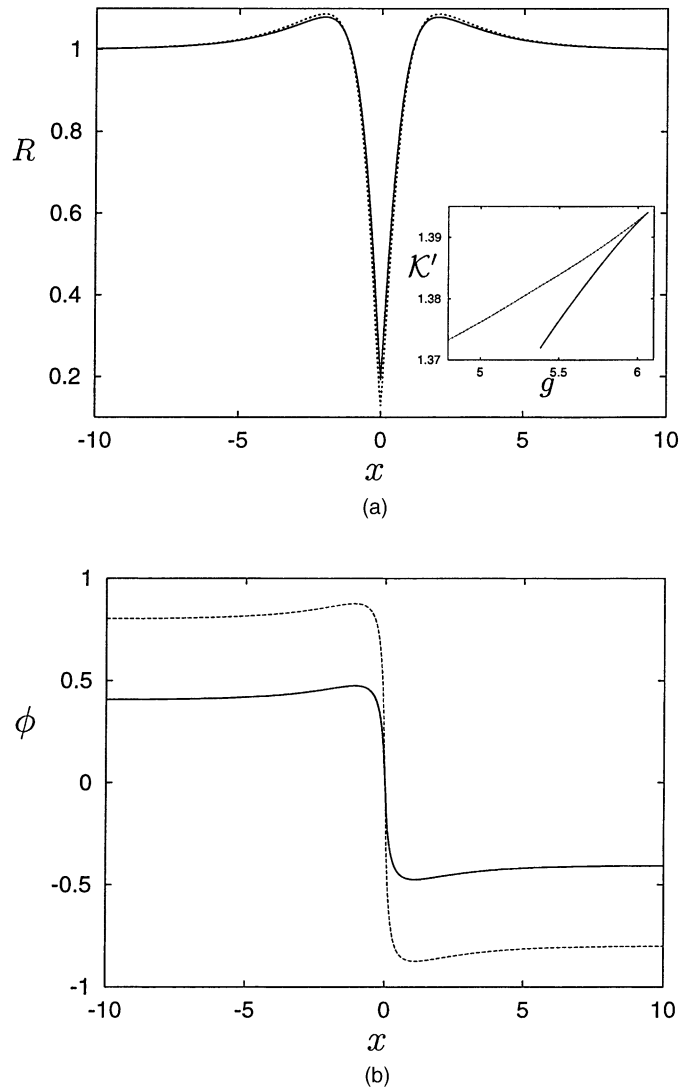


Fig. 7. (a) Modulus R of the stable (—) and unstable (---) stationary solutions to Eq. (59) for $g = 5.53$, $v = 0.15$, $q = 0.5$. Insert shows energy functional \mathcal{K}' of the stationary solutions versus g for $v = 0.15$ (see Eq. (58)); lower branch—energetically stable branch, upper branch—energetically unstable branch. The bifurcation occurs at $g = 6.06222$. (b) Phase ϕ of the stable (—) and unstable (---) stationary solutions, same conditions as in (a).

Thus, in sharp contrast with the uncharged Schrödinger flow (see Section 2.3), the eigenmodes pass uniformly from one branch of stationary solutions to the other. This is identical to what was observed in the sine-Gordon model (see Section 3.3).

4.4. Dynamical results

The method used to study numerically the dynamics of the system is the same as in Section 2.4, with $\Delta x = 0.05$ and $\Delta t = 0.001$.

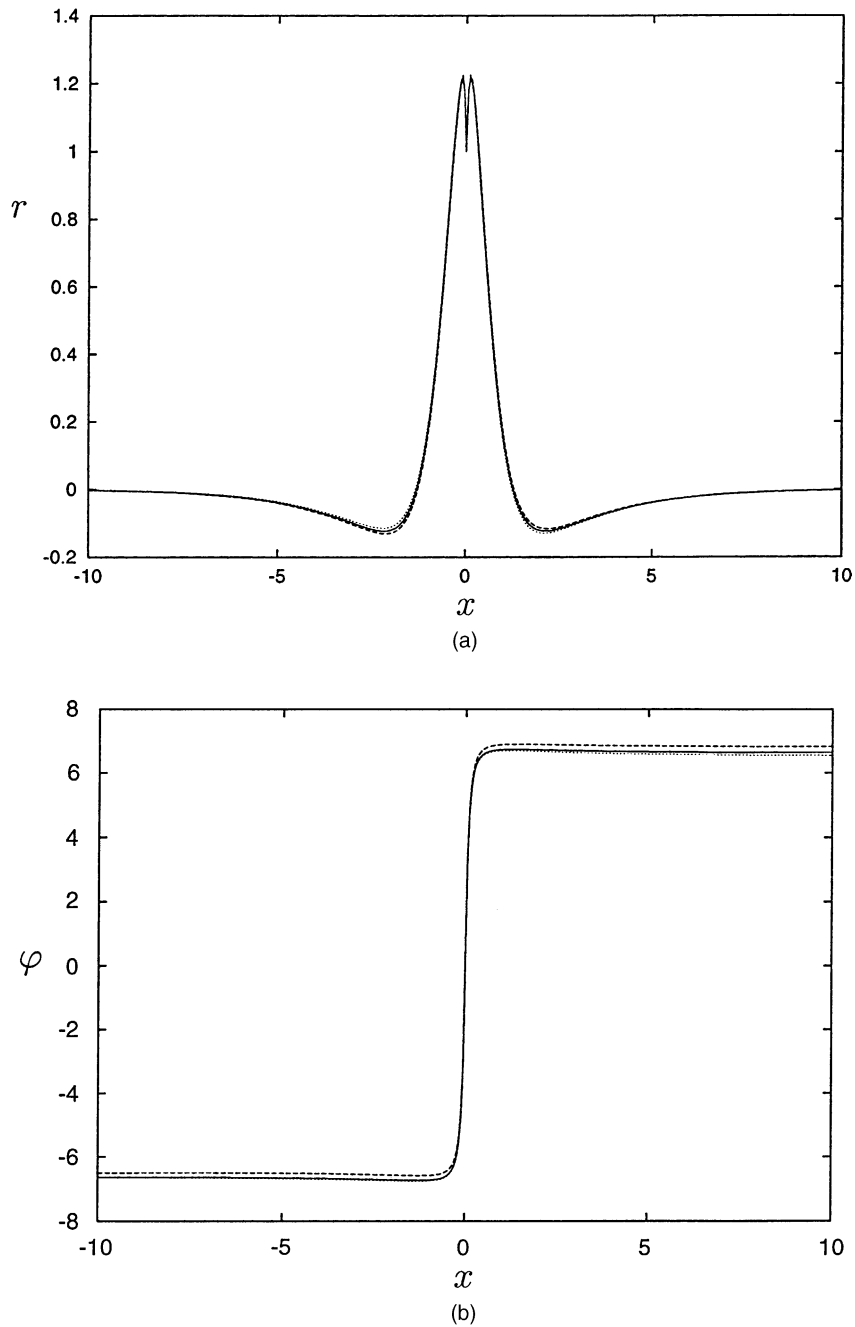


Fig. 8. Eigenmodes of (59). (a) Modulus r for $\nu = 0.15$ and $q = 0.5$ of the neutral mode (—) corresponding to $g = g_c = 6.06222$ and of a stable and an unstable eigenmodes for $g = 6.0622$. (b) Phase φ of the same eigenmodes (same conditions as in (a)). Note the continuity of the modes past the bifurcation.

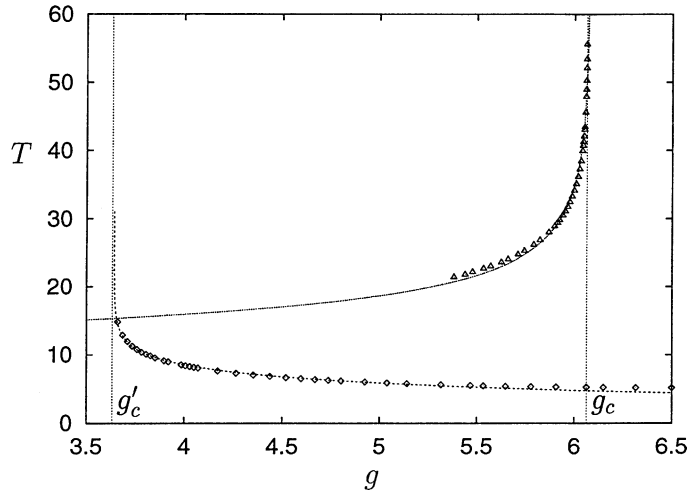


Fig. 9. Dynamical scalings close to the threshold ($g_c = 6.06222$, $g'_c = 3.64$, $v = 0.15$, $q = 0.5$). (Δ) Oscillations period on the stable branch, (\diamond) period of solitons emission. The curves represent fits with scaling laws $(g_c - g)^{-1/4}$ (\cdots), and $\log(g - g'_c)$ ($---$), see text.

Table 1

Dependence on q of the reduced subcritical interval $(g_c - g'_c)/g_c$

q	$(g_c - g'_c)/g_c$ (%)
1	48
0.5	40
0.25	33

Perturbing a stable stationary solution leads to collective oscillations around it, with no emission of sound waves, unlike the uncharged model. The period of the oscillations has been numerically calculated and is plotted in Fig. 9. It can be fitted by a scaling law of the form $T = \tau + \mu(g_c - g)^\lambda$, with $\lambda = -1/4$, which corresponds to the Hamiltonian saddle-node bifurcation (see Eq. (54)). Thus, as was already noticed above in Section 4.3, the system again behaves like the sine-Gordon pendulum chain of Section 3.

The system also exhibits subcriticality as in the Sine-Gordon model. For g greater than $g'_c < g_c$, a perturbed unstable stationary state yields a periodic emission of solitary waves. Fig. 9 shows the period, together with a fit to the scaling law $T = \tau - (1/\lambda)\log(g - g'_c)$. We thus find the same results as in the case of the sine-Gordon model, that is the scaling law of a homoclinic Andronov bifurcation.

Finally we studied the q dependence of the subcritical interval $(g_c - g'_c)/g_c$, by performing several series of runs. The results are summarized in Table 1. It can be seen by inspection of the table that this interval decreases with q . Note that the data is compatible with a $q^{1/4}$ scaling, a fit yielding the exponent 0.27.

5. Discussion and conclusion

5.1. Discussion

The purpose of the present section is to demonstrate that a very simple linear model exhibits some of the properties found in Sections 2 and 3. To wit, let us consider the following propagative equation

$$\partial_{tt}\psi - c^2(x)\partial_{xx}\psi + \omega_0^2\psi = 0, \quad (64)$$

with $c^2(x) = 1$ for $|x| > 1$ and $c^2(x) = -\gamma^2$ for $|x| < 1$.

For positive values of γ^2 , (64) presents an anti-propagative localized instability. Furthermore, if $\omega_0 \neq 0$, there is a gap in the dispersion relation of waves propagating far away from the region of the instability.

We are interested in symmetric solutions that display temporal instability. Setting $\psi(x, t) = e^{\lambda t}\phi(x)$, the solution reads

$$\phi(x) = A \cos \left[\frac{(\omega_0^2 + \lambda^2)^{1/2}}{\gamma} x \right], \quad \text{for } |x| < 1 \quad (65)$$

$$\phi(x) = B \exp[\mp(\omega_0^2 + \lambda^2)^{1/2}x], \quad \text{for } x \gtrless 1. \quad (66)$$

The continuity of $\phi(x)$ and $(d\phi/dx)(x)$ at $x = \pm 1$ implies

$$(\omega_0^2 + \lambda^2)^{1/2} = \gamma \arctan \gamma. \quad (67)$$

Suppose now that $\omega_0 = 0$. For $\lambda^2 > 0$ and $\gamma^2 > 0$, Eq. (67) becomes

$$\lambda = \gamma \arctan \gamma, \quad (68)$$

thus for $\gamma \ll 1$, one obtains after linearization $\lambda = \gamma^2 + o(\gamma^2)$.

Note that the linear relation between λ and γ^2 yields a damped ($\lambda < 0$) mode for negative γ^2 . However, the corresponding eigenmode (65) and (66) is spatially unbounded. This situation is somewhat similar to that of the so-called Gamov states, describing the decay of metastable states by quantum tunneling [29,30].

When γ^2 is negative (64) is propagative, even in the region $|x| < 1$. Because of this, the damping can also be understood through an optical analogy: waves, trapped inside a medium of index $1/|\gamma|$ lying at $|x| < 1$, and undergoing multiple reflections at the interfaces with a medium of index 1 for $|x| > 1$. A propagative wave in the center of the system $\psi(x, t) = e^{i(k_1x - \omega t)}$, of wave vector $k_1 \sim |\gamma|$, is partially reflected and transmitted with a ratio of wave amplitudes given by the transmission rate $\mathcal{T} = 4k_1k_2/(k_1 + k_2)^2 \sim |\gamma|$ (with k_2 the wave vector of the transmitted wave of order unity). In a unit time, the wave reflects $\mathcal{N} \sim 1/c \sim |\gamma|$ times at the interface, yielding a decay rate $\lambda \sim \mathcal{N}\mathcal{T} \sim \gamma^2$; this argument reproduces the expected scaling law $\lambda \sim \gamma^2$.

Suppose now that $\omega_0 \neq 0$. The instability takes place when $\lambda = 0$, and Eq. (67) becomes

$$\omega_0 = \gamma \arctan \gamma. \quad (69)$$

Let $\gamma^2 = \gamma_0^2 + \xi$, where γ_0 verifies (69), then one finds, after linearizing in ξ (67)

$$\frac{1}{2\omega_0}\lambda^2 = \frac{1}{2\gamma_0} \left(\frac{\gamma_0}{1 + \gamma_0^2} + \arctan \gamma_0 \right) \xi, \quad (70)$$

thus, a scaling law of the form $\lambda^2 \sim \xi$. Note that λ^2 scales linearly in the variation of γ^2 in sharp contrast with the case $\omega_0 = 0$. Also note that the eigenvector (65) and (66) is bounded both for stable and unstable values of γ^2 .

The drastic effect of ω_0 on both the difference in scaling laws and in continuity of eigenmodes is reminiscent of the differences found in Sections 2 and 3. It thus seems reasonable to infer that these effects are typical of situations with localized instabilities in infinitely extended domains.

5.2. Conclusion

The three models studied in this paper are all spatially extended Hamiltonian systems exhibiting a transition to dissipation. Beyond a critical threshold, they start radiating energy to infinity by emitting solitary waves (kink and

anti-kink in the case of the sine-Gordon equation, gray solitons or waves alike in the case of the NLSE). However, two *distinct* mechanisms have been encountered.

In the case of the uncharged nonlinear Schrödinger flow, the transition takes place through a usual saddle-node Andronov bifurcation. Although the system is Hamiltonian, it behaves like a dissipative system because its dynamics is coupled with the emission of sound waves. In this case, the dispersion relation

$$\omega = vk + \sqrt{2k^2 + k^4} \quad (71)$$

is gapless so that sound waves of arbitrarily low frequency can, indeed, propagate. This fact is related to the $\delta^{1/2}$ dynamical scaling, characteristic of dissipative systems. There is no hysteresis in this case.

In contrast, the sine-Gordon model and the charged nonlinear Schrödinger flow share a different behavior; the transition takes place through a Hamiltonian saddle-node bifurcation, characterized by a $\delta^{1/4}$ dissipation-less scaling law. The dispersion relations of these two systems are

$$\omega^2 = \omega_c^2 + k^2, \quad \text{with } \omega_c = 1, \quad (72)$$

$$\omega = vk + \sqrt{\omega_c^2 + 2k^2 + k^4}, \quad \text{with } \omega_c = q. \quad (73)$$

Thus, no wave can propagate below the cut-off frequency ω_c , in contrast to the uncharged NLS system. We found that the periodic emission of solitary waves exhibits subcriticality and log scaling characteristic of a homoclinic Andronov bifurcation.

The charged nonlinear Schrödinger flow model confirmed the genericity of this behavior by adding to the dispersion relation of the nonlinear Schrödinger flow a tunable gap. The interval of subcriticality was found to decrease with the gap.

The simple linear model introduced in Section 5.1 allowed us to understand some of the effects of the gap, such as the existence of Gamov states on the stable branch in the gapless case. However, this linear model bears no direct relation with the linear stability equations (20), (21) and (48). In the gapless case, a remarkable fact is that the linearized stability equations display genuine irreversible behavior on the stable branch.

A challenge, left for further study, is to derive from the original time-reversible equation of motion an irreversible normal form of the type (36). Another point, that we will study in the future, is the generalization of the above 1D results to 2D and 3D systems. Irreversible scaling is known to occur in gapless 2D systems [10,11] but the behavior of the eigenmodes close to the bifurcation is still unknown.

Acknowledgements

We wish to thank T.J. Bridges for pointing out to us the exact solution (50) and the compound matrix method of [15,16]. We also acknowledge helpful scientific discussion with M. Argentina, P. Coullet, V. Hakim, E. Tirapegui and L. Tuckerman.

References

- [1] R.J. Donnelly, *Quantized Vortices in Helium II*, Cambridge University Press, Cambridge, 1991.
- [2] E.P. Gross, Structure of a quantized vortex in boson systems, *Nuovo Cimento* 20 (3) (1961).
- [3] L.P. Pitaevskii, Vortex lines in an imperfect Bose gas, *Sov. Phys. JETP* 13 (2) (1961).
- [4] L.D. Landau, E.M. Lifshitz, *Fluid Mechanics*, 2nd Edition, Butterworths/Heinemann, London, 1995.
- [5] F. Dalfovo, S. Giorgini, L.P. Pitaevskii, S. Stringari, Theory of Bose–Einstein condensation in trapped gases, *Rev. Mod. Phys.* 71 (3) (1999).

- [6] C. Raman, M. Köhl, R. Onofrio, D.S. Durfee, C.E. Kuklewicz, Z. Hadzibabic, W. Ketterle, Evidence for a critical velocity in a Bose–Einstein condensed gas, *Phys. Rev. Lett.* 83 (13) (1999) 2502–2505.
- [7] T. Frisch, Y. Pomeau, S. Rica, Transition to dissipation in a model of superflow, *Phys. Rev. Lett.* 69 (1992) 1644–1647.
- [8] Y. Pomeau, S. Rica, Vitesse limite et nucléation dans un modèle de superfluide, *C.R. Acad. Sci. (Paris), Série II* 316 (1993) 1523.
- [9] V. Hakim, Nonlinear Schrödinger flow past an obstacle in one dimension, *Phys. Rev. E* 55 (3) (1997) 2835–2845.
- [10] C. Huepe, M.-É. Brachet, Solutions de nucléation tourbillonnaires dans un modèle d’écoulement superfluide, *C.R. Acad. Sci. (Paris), Série II* 325 (1997) 195–202.
- [11] C. Huepe, M.-É. Brachet, Scaling laws for vortical nucleation solutions in a model of superflow, *Physica D* 140 (1–2) (2000) 126–140.
- [12] J. Guckenheimer, P. Holmes, *Nonlinear Oscillations, Dynamical Systems and Bifurcations of Vector Fields*, Springer, Berlin, 1983.
- [13] M. Argentina, *Dynamique des systèmes bistables spatialement étendus*, Ph.D. Thesis, Université de Nice-Sophia Antipolis, 1999.
- [14] M. Argentina, P. Couillet, L. Mahadevan, Colliding waves in a model excitable medium: preservation, annihilation and bifurcation, *Phys. Rev. Lett.* 79 (15) (1997) 2803–2806.
- [15] A.L. Afendikov, T.J. Bridges, Instability of the Hocking-Stewartson pulse and its implications for three-dimensional Poiseuille flow, *Proc. R. Soc. Lond. A* 457 (2001) 257–272.
- [16] L. Allen, T.J. Bridges, Numerical exterior algebra and the compound matrix method, *Numer. Math.*, 2001, in press.
- [17] C. Nore, M. Abid, M.-É. Brachet, Decaying Kolmogorov turbulence in a model of superflow, *Phys. Fluids* 9 (9) (1997) 2644–2669.
- [18] T. Tsuzuki, Nonlinear waves in the Pitaeviskii–Gross equation, *J. Low Temp. Phys.* 4 (4) (1971).
- [19] V.E. Zakharov, A.B. Shabat, Interaction between soliton in a stable medium, *Sov. Phys. JETP* 37 (5) (1973) 823–828.
- [20] S. Lang, *Algebra*, 3rd Edition, Addison-Wesley, Reading, MA, 1992.
- [21] W.H. Press, S.A. Teukolsky, W.T. Vetterling, B.P. Flannery, *Numerical Recipes*, 2nd Edition, Cambridge University Press, Cambridge, 1992 (Chapter 9).
- [22] P.G. Drazin, W.H. Reid, *Hydrodynamic Stability*, Cambridge University Press, Cambridge, 1981.
- [23] I.V. Barashenkov, Stability criterion for dark solitons, *Phys. Rev. Lett.* 77 (1996) 1193–1197.
- [24] M. Remoissenet, *Waves Called Solitons, Concepts and Experiments*, 2nd Edition, Springer, Berlin, 1994.
- [25] D.W. McLaughlin, A.C. Scott, Perturbation analysis of fluxon dynamics, *Phys. Rev. A* 18 (4) (1978) 1652–1680.
- [26] A.S. Alexandrov, W.H. Beere, Collective excitations and screening properties of a condensed charged Bose gas, *Phys. Rev. B* 51 (9) (1995) 5887–5891.
- [27] R.P. Feynman, *Statistical Mechanics, a Set of Lectures*, Benjamin/Cummings, Menlo Park, CA, 1972.
- [28] M. Abid, M. Brachet, F. Debbasch, C. Nore, Galilean and relativistic nonlinear wave equations: an hydrodynamical tool? In: E. Tirapegui, W. Zeller (Eds.), *Instabilities and Nonequilibrium Structures V*, Kluwer Academic Publishers, Dordrecht, 1996, pp. 33–52.
- [29] L. Landau, E. Lifshitz, *Quantum Mechanics*, 3rd Edition, Butterworths/Heinemann, London, 1997.
- [30] C.J. Joachain, *Quantum Collision Theory*, North-Holland, Amsterdam, 1975.